JMEPEG (2017) 26:4046–4055
DOI: 10.1007/s11665-017-2819-z

1059-9495/$19.00

Microstructure, Mechanical and Wear Behaviors of Hot-Pressed Copper-Nickel-Based Materials for Diamond Cutting Tools

G. Miranda, P. Ferreira, M. Buciumeanu, A. Cabral, M. Fredel, F.S. Silva, and B. Henriques

(Submitted November 2, 2016; in revised form April 16, 2017; published online July 21, 2017)

The current trend to replace cobalt in diamond cutting tools (DCT) for stone cutting has motivated the study of alternative materials for this end. The present study characterizes several copper-nickel-based materials (Cu-Ni; Cu-Ni-10Sn, Cu-Ni-15Sn, Cu-Ni-Sn-2WC and Cu-Ni-Sn-10WC) for using as matrix material for diamond cutting tools for stone. Copper-nickel-based materials were produced by hot pressing, at a temperature of 850 °C during 15 min and under an applied pressure of 50 MPa. The mechanical properties were evaluated though the shear strength and hardness values. The microstructures and fracture surfaces were analyzed by SEM. The wear behavior of all specimens was assessed using a reciprocating ball-on-plate tribometer. The hot pressing produced compacts with good densification. Sn and WC promoted enhanced mechanical properties and wear performance to Cu-Ni alloys. Cu-Ni-10Sn and Cu-Ni-10Sn-2WC displayed the best compromise between mechanical and wear performance.

Keywords Cu-Ni alloys, diamond cutting tools, hot pressing, mechanical properties, microstructure, wear

1. Introduction

Stone cutting tools are made of abrasive reinforcements embedded in a metallic matrix, with a common solution being the use of diamond-reinforced metals (Ref 1). These tools work in severe in-service conditions (Ref 2), and therefore an appropriate selection of a suited matrix along with an effective reinforcement is mandatory, once the tool performance will be dictated by their constituents.

Regarding diamond cutting tools, the diamond-embedded particles are responsible for the cutting process, while the metal matrix must withstand the forces and attrition generated during the cutting process. However, the wear rate of the matrix must be similar to the wear rate of the diamond particles in order to allow their replacement when the particles are blunt, e.g., lost their abrasiveness (Ref 3). By guarantying this renovation of the reinforcing particles, these tools are able to present a constant cutting rate, because the continuous metal matrix wear causes new diamond particles to emerge, freeing up those which during the cutting process lost their sharp edges.

Additionally, the metal matrix must present a chemical and physical interaction with the diamond particles, being able to retain them during the cutting process (Ref 1) and also preserving the diamond properties. The diamond cutting tools industry uses mainly two powder metallurgy techniques for producing these tools: hot pressing (HP) [more common (Ref 4)] or cold pressing followed by sintering in vacuum furnace (Ref 1).

HP consists in the simultaneous application of temperature and pressure in order to sinter a metal matrix in order to get a product free of porosity, being used for a wide range of materials (Ref 5-9). When used for producing diamond-reinforced metals, HP presents the advantage to strictly control the processing parameters (temperature, pressure and time) in order to avoid the dissolution and/or graphitization of diamond particles, fact that can hamper the tool performance. Another benefit from using HP is the ease of mixing different powders and consequently the possibility of creating new composite materials with appropriate physical and mechanical properties. This technique brings also an enormous freedom in the parts design, once they can be used for obtaining intricate geometries (Ref 1, 10) and near net shape parts.

The diamonds used for fabricating these tools are synthetic and therefore withstanding temperatures till 900 °C without degradation. In this sense, diamond cutting tools are mostly produced by powder metallurgy techniques using sintering temperatures between 700 and 900 °C (Ref 10).

Regarding the metal matrices, and given the target properties listed above, the most commonly used are cobalt- and iron-based alloys (Ref 11). Some alloying elements are usually added to these matrices, like tin (Sn) and tungsten (W) (Ref 12), besides being frequently reinforced by tungsten carbide (WC) (Ref 11). These additions are made in order to obtain a matrix with higher mechanical and/or wear performance, as well as to improve the retention of the diamond particles.

G. Miranda, P. Ferreira, and **F.S. Silva**, Center for Micro-Electro Mechanical Systems (CMEMS-UMinho), University of Minho, Campus de Azurém, 4800-058 Guimarães, Portugal; **M. Buciumeanu**, Cross–Border Faculty of Humanities, Economics and Engineering, University of Galati, Dunarea de Jos, Domneasca 47, 800008 Galați, Romania; **A. Cabral** and **M. Fredel**, Ceramic and Composite Materials Research Group (CERMAT), Federal University of Santa Catarina (UFSC), Campus Trindade, Florianópolis, SC, Brazil; and **B. Henriques**, Center for Micro-Electro Mechanical Systems (CMEMS-UMinho), University of Minho, Campus de Azurém, 4800-058 Guimarães, Portugal; and Ceramic and Composite Materials Research Group (CERMAT), Federal University of Santa Catarina (UFSC), Campus Trindade, Florianópolis, SC, Brazil. Contact e-mail: gmiranda@dem.uminho.pt.

Cobalt is one of the most commonly used matrix, once it presents perfect compatibility with diamond when using adequate processing temperatures; grants a suitable retention of diamond particles and its wear resistance is considered adequate for these in-service conditions (Ref 13). Despite these good features, Co is a highly toxic material and its availability is reduced (Ref 13). In this context, there is a need to find metallic materials than can replace Co in these tools (Ref 14). Iron-based alloys have been studied as alternative, however when using these alloys, graphitization of the diamond particles during sintering can occur, thus reducing the lifespan of these tools (Ref 14).

Copper (Cu) low melting point (when compared with Co and Fe) is a great advantage to avoid diamond particles graphitization. Carbon null solubility in copper is another advantage, once it guaranties that diamond particles retain their properties after processing. However, Cu displays lower hardness relative to cobalt- or iron-based alloys, which is a drawback. This aspect can be somewhat overcome by adding nickel (Ni), thus obtaining a Cu-Ni alloy, with higher mechanical properties than Cu (Ref 15). Furthermore, the addition of WC in adequate amounts has been proven effective by increasing hardness and wear resistance (Ref 16). Sn has also been added to Cu-Ni and other alloys (Ref 17) once due to its low melting temperature, densification is enhanced by liquid-phase sintering (Ref 17), leading to higher mechanical properties and improved retention of diamond particles.

This work intends to assess the viability of using Cu-Ni alloys as matrix for diamond cutting tools. For this purpose, several materials were produced and characterized when regarding mechanical properties and wear behavior.

2. Experimental Details

2.1 Specimens Fabrication

Copper-nickel-based specimens were produced starting from elemental copper (Cu) and nickel (Ni) powders. Cu and Ni were mixed using 55 wt.% of Cu. Tin (Sn) and Tungsten Carbide (WC) were added to the Cu and Ni mixture, thus obtaining single reinforced materials and also double reinforced materials. Table 1 summarizes the size and supplier of all the powders used to produce these specimens. Table 2 shows the composition of the produced specimens.

The elemental powders were mechanically mixed in a blender for 6 h. The obtained mixture was divided and placed inside graphite dies, with 10 mm width and 30 mm length. The composites were then sintered by means of pressure-assisted sintering process, in vacuum, using a high-frequency induction furnace (schematically represented in Fig. 1), according to the following procedure. The die was placed inside the chamber, while the sample was compressed at 8 MPa, and then heated up to 800 °C, with a heating rate of 25 °C/min. When the temperature reached 800 °C the pressure on the sample was raised to 50 MPa (while the heating proceeds at 25 °C/min till 850 °C). The sample was maintained at 850 °C with 50 MPa pressure, for 15 min. Afterward, the samples were allowed to cool inside the die, in vacuum, till room temperature. The obtained samples had a diameter of 10 mm and a height of 10 mm.

2.2 Chemical Characterization

The obtained specimens were characterized in terms of chemical composition by means of *Scanning Electron Microscopy (SEM)/Energy Dispersive Spectrometer (EDS)*. The fracture surfaces (after shear tests) were also obtained by means of *SEM*.

2.3 Hardness Measurements

Vickers Hardness measurements were conducted in the produced specimens using an EMCO-TEST, DuraScan model, hardness tester was used, with a dwell time of 15 s under a load of 200 gf.

2.4 Shear Tests

Shear tests were performed at room temperature (~23 °C), with a crosshead speed of 0.02 mm/s, in a servohydraulic machine (Instron 8874), equipped with a 25 kN capacity load cell. Tests were performed in a custom-made stainless steel apparatus with a sliding part equipped with a cutting tool. A compressive force was applied in the sliding part in order to promote fracture due to shear loading. Shear strength (MPa) was calculated dividing the highest force (N) recorded during the test by the cross section area (mm^2).

2.5 Wear Tests

A reciprocating ball-on-plate tribometer (Bruker-UMT-2) was used to evaluate the wear behavior of the produced materials. Reciprocating sliding tests were performed using a 20-N normal load, 1 Hz and a 6-mm total stroke length during 60 min. The cylindrical specimens were cut for producing plates with 10 mm in diameter and 4 mm in height. Alumina

Table 2 Composition of the produced specimens

Specimens	Composition, in wt.%
Cu-Ni	55Cu-45Ni
Cu-Ni-10Sn	(55Cu-45Ni)-10Sn
Cu-Ni-15Sn	(55Cu-45Ni)-15Sn
Cu-Ni-Sn-2WC	(55Cu-45Ni)-10Sn-2WC
Cu-Ni-Sn-10WC	(55Cu-45Ni)-10Sn-10WC

Note on the compositions' calculations: Cu-Ni-10Sn stands for a composition of 90 wt.% * (55Cu-45Ni) + 10 wt.% * Sn. The same procedures apply to the remaining compositions

Table 1 Size and supplier of the powders used for the production of the specimens

Material	Powder size, μm	Supplier
Cu	<44	JB Química Indústria e Comércio Ltda
Ni	3-6	Citra do Brasil Comércio Internacional Ltda
Sn	<44	JB Química Indústria e Comércio Ltda
WC	2-3	JB Química Indústria e Comércio Ltda

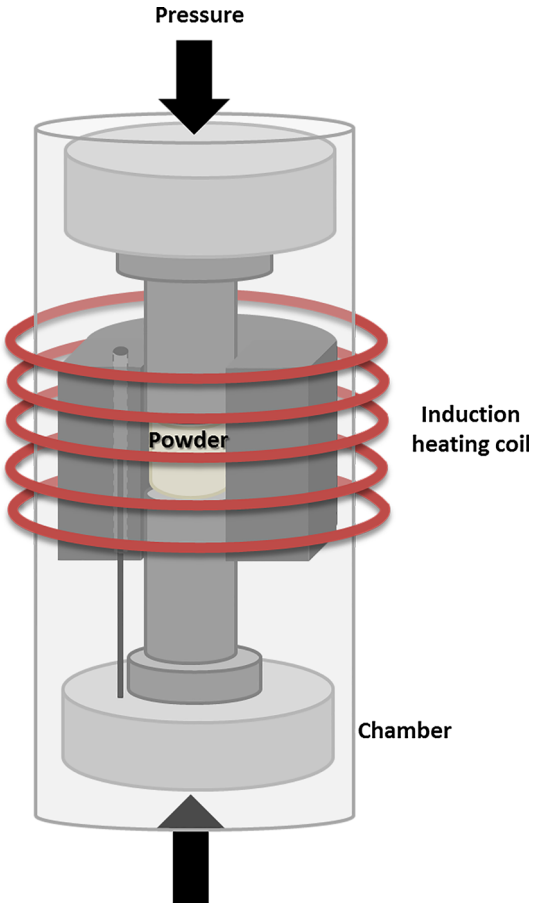

Fig. 1 Schematic representation of the hot-pressing sintering system

balls (with 10 mm diameter, from *Ceratec, NL*) were used as counterbody in these tests.

Both balls and pins were cleaned in an ultrasonic bath of isopropyl alcohol for 15 min before and after the tests. After testing, the weight loss was estimated by measuring the weight of the samples. All tests were performed in laboratory environment (20 ± 2 °C). The results were taken as the average from at least three tests.

The coefficient of friction (COF) was recorded automatically during the sliding test, using data acquisition software. The tribometer has a load cell that is measuring the frictional force, and the software has the formula of COF = frictional force/applied load. The plot of COF/friction force versus time/or sliding distance is shown in real time.

3. Results and Discussion

3.1 Microstructural and Chemical Characterization

SEM images of the produced specimens (Fig. 2) show that no porosity is found, assessing the effectiveness of the hot-pressing process for the production of these materials.

XRD analysis was performed in order to assess the formed compounds on the Cu-Ni matrix. Figure 3 shows that only CuNi peaks were detected.

In order to assess the reinforcement's dispersion and the possible reaction products between the Cu-Ni matrix and the elements/reinforcements used on these materials, a microstructural and chemical characterization was made by SEM/EDS (Fig. 3 and Table 3).

When analyzing Fig. 4(a) and (b) it is possible to verify that Cu-Ni-Sn specimens present a different microstructure than that found on Cu-Ni (Fig. 2a), with Sn being easily found on

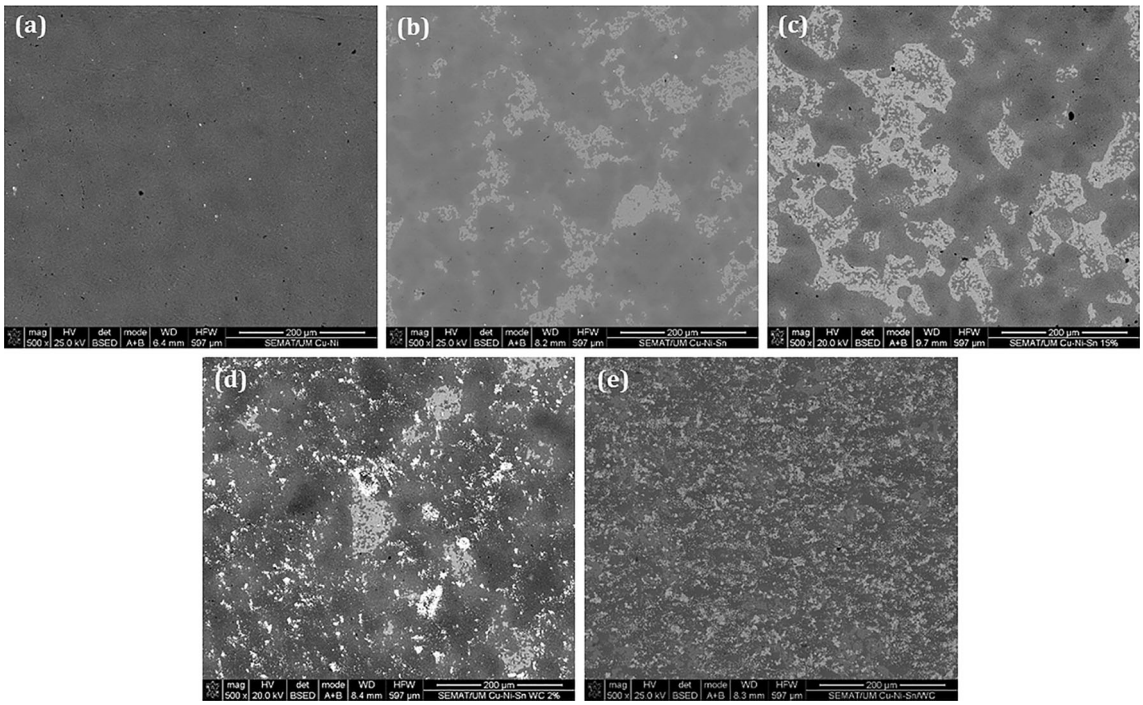

Fig. 2 SEM images of (a) Cu-Ni; (b) Cu-Ni-10Sn; (c) Cu-Ni-15Sn; (d) Cu-Ni-Sn-2WC and (e) Cu-Ni-Sn-10WC

specific areas (see Z1 zones on Fig. 4a and b). Due to the fact that Sn has a melting temperature of 231.9 °C (Ref 18), during the hot-pressing stage (850 °C), liquid-phase sintering occurs. Due to this fact, the presence of Sn is known to improve the densification of the material (Ref 17), once it undergoes melting, thus hindering the presence of any residual porosity on these specimens.

Regarding Cu-Ni-10Sn-WC specimens, reinforced with WC particles having 2 to 3 micrometers, Fig. 4(c) and (d) shows the formation of WC clusters. These images show that WC is not wetted by liquid Sn during sintering, once no WC is found inside Sn areas (see Z2 zones on Fig. 4c and d). No reaction between the WC and Cu-Ni-Sn was detected, as expected and reported by other studies (Ref 19, 20) where WC limited solubility in copper and an extremely low tendency to form interfacial intermetallic with copper alloys is proven.

3.2 Mechanical Properties

Hardness and shear strength results experimentally obtained for all the materials produced in this work are shown in Fig. 5.

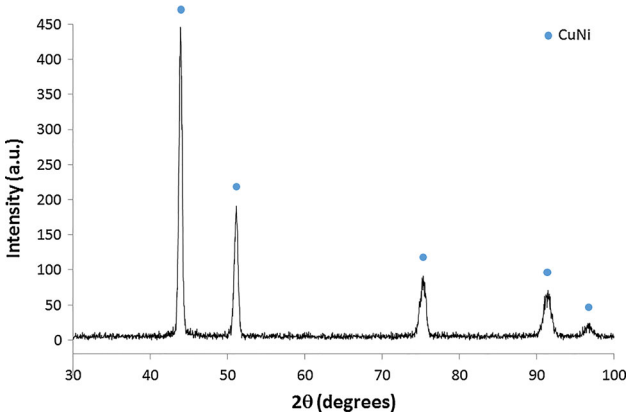

Fig. 3 XRD pattern for Cu-Ni specimen

The representative load-displacement curves obtained from shear tests are presented in Fig. 6. Regarding Cu-Ni specimen's hardness and shear strength, a good accordance with values found on literature for CuNi phase was verified (Ref 21). The addition of Sn to Cu-Ni (Cu-Ni-10Sn and Cu-Ni-15Sn) has led to an increase in hardness and shear strength, as reported by other authors in several alloys (Ref 17). When increasing the Sn content from 10 to 15%, a hardness increase was verified, although shear strength exhibited similar values. Liquid-phase sintering (due to Sn melt) can explain these results due to a higher densification by eliminating residual porosity (Ref 17).

Regarding specimens with simultaneous addition of Sn and WC (Cu-Ni-Sn-2WC and Cu-Ni-Sn-10WC) it is possible to verify that hardness and shear strength although superior to those of Cu-Ni were lower than the values attained by Cu-Ni-10Sn and Cu-Ni-15Sn. This outcome can be explained by the fact that WC particles have 2 to 3 micrometers, and thus are prone to agglomerate, forming clusters that lead to a reduction on hardness and shear strength.

After shear tests, the specimens fracture surfaces were examined using SEM (Fig. 7 and 8). Macroscopically, it is possible to see a clear difference in the fracture topography between Cu-Ni (Fig. 7a); the Cu-Ni-Sn specimens (Fig. 7b and c) and the Cu-Ni-Sn-WC group (Fig. 7d and e). While Cu-Ni specimens exhibited a typical ductile fracture, shown by an expressive plastic deformation (Fig. 8a), Cu-Ni-Sn specimens (especially Cu-Ni-15Sn (Fig. 8b) exhibited the most brittle fracture among these materials. By analyzing Cu-Ni-15Sn fracture surface (Fig. 8b) two different areas can be found: ones where a ductile behavior is prevalent, corresponding to CuNi (see backscattered image on Fig. 8b), and others with a more fragile fracture, corresponding to Sn rich areas. These observations are aligned with the mechanical properties obtained for Cu-Ni-15Sn, being the harder material, with one of the highest shear strength. Regarding Cu-Ni-Sn-WC specimens, ductile fractures were observed, as shown in Fig. 8(c), where the WC clusters mentioned above are clearly visible.

Table 3 Chemical composition of marked zones in Fig. 4, obtained by EDS

Composition, wt.%	Cu-Ni-10Sn	Cu-Ni-15Sn	Cu-Ni-Sn-2WC	Cu-Ni-Sn-10WC
Z1				
Cu	14.95	17.81	16.18	16.83
Ni	47.11	41.03	42.79	43.15
Sn	37.94	39.38	38.09	36.22
O	…	1.79	…	…
W	…	…	1.32	…
C	…	…	1.63	3.80
Z2				
Cu	31.10	29.64	2.30	64.36
Ni	53.86	56.94	97.70	23.82
Sn	13.99	13.42	…	7.00
O	1.06	…	…	…
W	…	…	…	…
C	…	…	…	4.81
Z3				
Cu	…	…	2.39	4.38
Ni	…	…	2.28	4.08
Sn	…	…	…	…
O	…	…	…	…
W	…	…	89.98	81.79
C	…	…	5.35	9.75

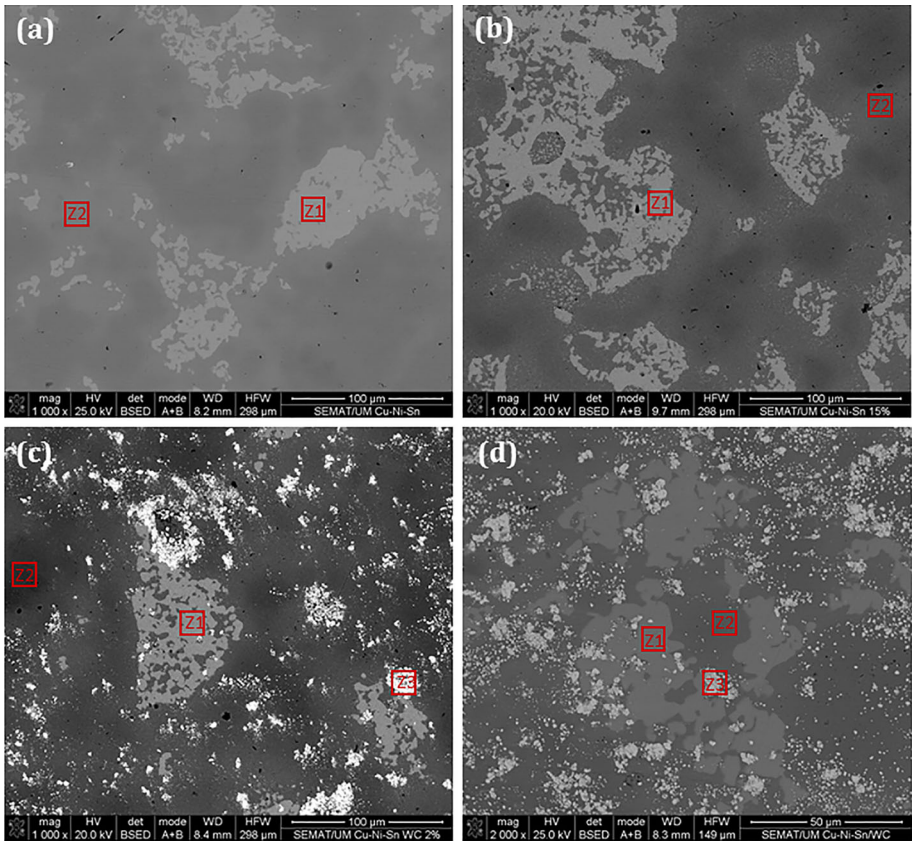

Fig. 4 SEM images with marked zones for EDS analysis of (a) Cu-Ni-10Sn; (b) Cu-Ni-15Sn; (c) Cu-Ni-Sn-2WC and (d) Cu-Ni-Sn-10WC, with marked zones for EDS analysis

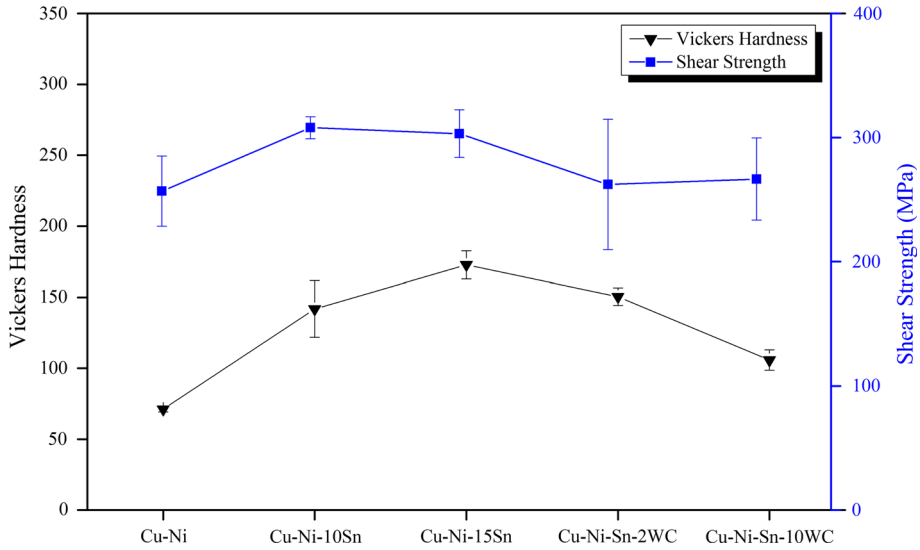

Fig. 5 Hardness and shear strength obtained for the produced materials

3.3 Wear Behavior

3.3.1 Weight Loss. The average weight loss obtained for Cu-Ni, Cu-Ni-10Sn, Cu-Ni-15Sn, Cu-Ni-Sn-2WC and Cu-Ni-Sn-2WC is shown in Fig. 9. When analyzing these results it is possible to conclude that adding Sn or/and WC to Cu-Ni led to a decrease on weight loss of these materials, thus rising their wear resistance.

The results concerning weight loss were found coherent with the measured hardness (Fig. 5), with the material having lower hardness displaying the highest weight loss (Cu-Ni). The materials that presented greater resistance to wear were Cu-Ni-10Sn, Cu-Ni-Sn-2WC and Cu-Ni-15Sn (Fig. 9), corresponding to the hardest materials. Comparing to Cu-Ni, Cu-Ni-10Sn presented an expressive 96% reduction on the wear rate, Cu-Ni-Sn-2WC displayed a 94% reduction, while Cu-Ni-15Sn exhibited an 84% reduction on the weight loss. Regarding Cu-Ni-Sn-10WC only a 52% reduction on the weight loss was verified. Additions of dispersed hard particles in DCTs metallic

matrices have been used with the purpose of controlling the matrix material wear rate (Ref 1, 22, 23). In this work, while WC particles were protecting the material from wear (and thus lowering the weight loss), the presence of WC clusters, especially on Cu-Ni-Sn-10WC, can explain this material lower wear performance.

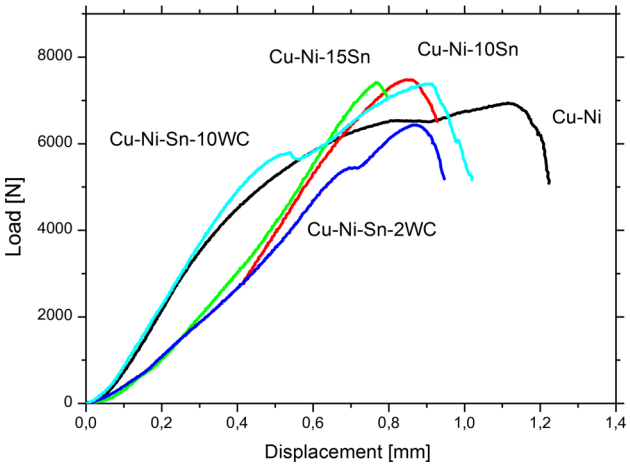

Fig. 6 Load-displacement curves obtained from the shear tests of the produced materials

3.3.2 Coefficient of Friction. Figure 10 shows the evolution of the coefficient of friction (COF) with sliding distance for Cu-Ni, Cu-Ni-10Sn, Cu-Ni-15Sn, Cu-Ni-Sn-2WC and Cu-Ni-Sn-10WC, during the reciprocating sliding tests, against alumina balls.

For all the performed tests, a typical evolution of the COF with sliding distance was verified: a first period corresponding to the running-in regime after which the COF enters in a steady-state conditions remaining approximately constant during the whole test. Table 4 shows the average values obtained for the COF (after the running-in stage) for Cu-Ni, Cu-Ni-10Sn, Cu-Ni-15Sn, Cu-Ni-Sn-2WC and Cu-Ni-Sn-2WC, showing no significant differences between them.

3.3.3 Wear Track Analysis. SEM images and corresponding backscattered (BSE) images of the worn surfaces of Cu-Ni; Cu-Ni-10Sn; Cu-Ni-15Sn; Cu-Ni-Sn-2WC and Cu-Ni-Sn-10WC after sliding against unreinforced alumina ball are shown in Fig. 11.

From Fig. 11 it is possible to conclude that the track with greater width was observed for Cu-Ni, corresponding to the material with higher weight loss. Conversely, the track with

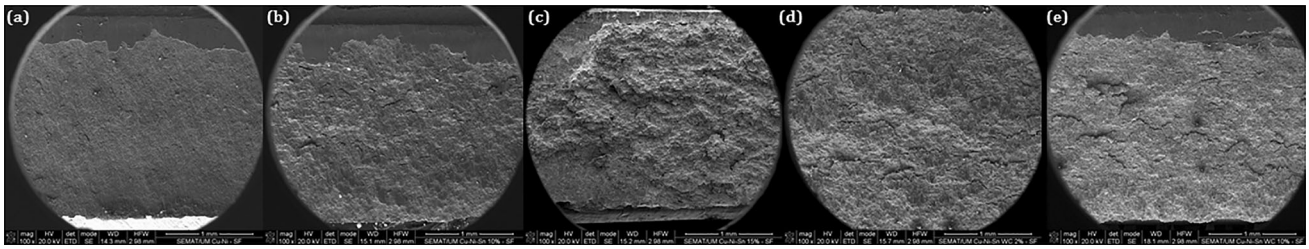

Fig. 7 Fracture surfaces of (a) Cu-Ni; (b) Cu-Ni-10Sn; (c) Cu-Ni-15Sn; (d) Cu-Ni-Sn-2WC and (e) Cu-Ni-Sn-10WC

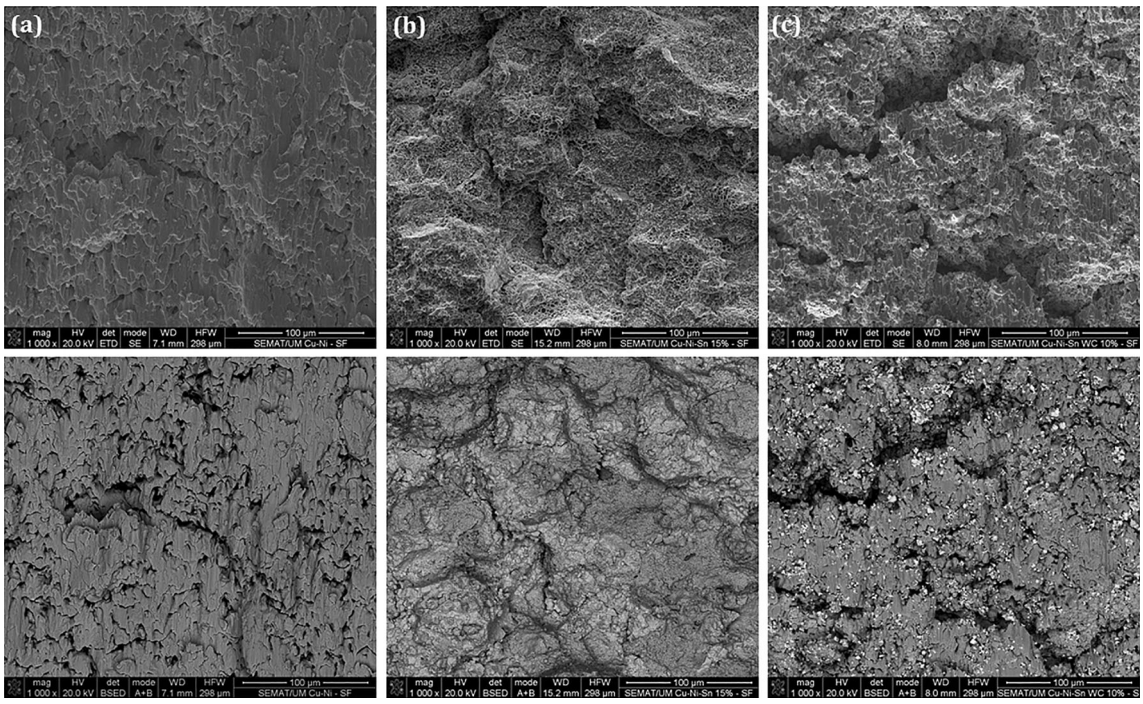

Fig. 8 Detail views of the fracture surfaces of (a) Cu-Ni; (b) Cu-Ni-15Sn and (c) Cu-Ni-Sn-10WC

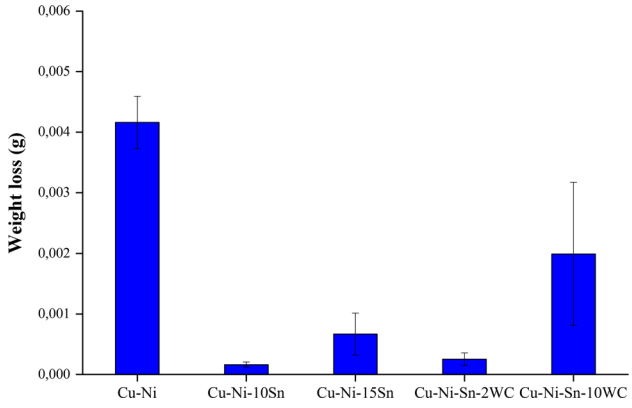

Fig. 9 Weight loss after reciprocating wear tests of the produced materials against alumina ball

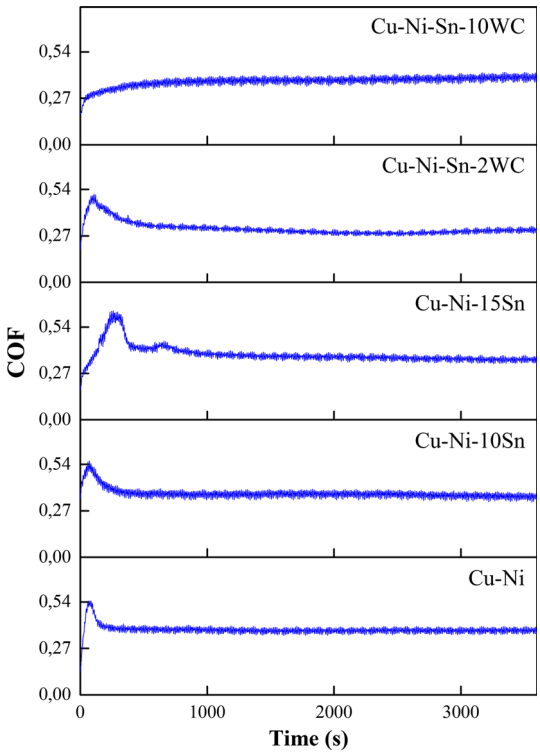

Fig. 10 COF evolution with sliding distance for the produced materials against alumina ball

Table 4 Average COF values for the produced materials against alumina ball

Material	COF
Cu-Ni	0.324
Cu-Ni-10Sn	0.371
Cu-Ni-15Sn	0.393
Cu-Ni-Sn-2WC	0.346
Cu-Ni-Sn-10WC	0.368

lower width was found for Cu-Ni-10Sn, material presenting the lower weight loss.

In order to understand the dominant wear mechanisms in each of the tested materials, detailed backscattered (BSE) images of the worn surfaces were acquired and the chemical compositions of several areas were determined.

Starting by the wear track of Cu-Ni (Fig. 12a) it is possible to verify that a significant plastic deformation occurred, with visible grooves, due to the sliding of the alumina ball (marked with Z2 in Fig. 12a). Additionally, some material detachment areas, due to adhesion wear, were found on this track, marked with Z1 in Fig. 12a. In fact, while Z1 composition presents only Cu and Ni, corresponding to freshly exposed areas, Z2 zone shows the presence of alumina ball debris besides some oxidation (due to the noteworthy oxygen content), generated due to frictional heating on this material that is not detached, but instead plastically deformed (see Table 5).

Regarding Cu-Ni-10Sn, similar observations were made, with significant plastic deformation along the sliding direction and also detachment areas (Fig. 12b). The main difference is in the depth of the detached areas that are significantly lower in Cu-Ni-10Sn, when comparing with Cu-Ni, as clearly shown by the magnified images of the wear tracks found in Fig. 13(a) and (b).

Concerning Cu-Ni-15Sn, only slight grooves were detected (Fig. 13c). However, innumerous cracks from tensile stresses during plowing were detected (Fig. 13c), besides adhesion wear sites. This material revealed a lower plastic deformation, fact that can be directly correlated with the higher hardness displayed by the Cu-Ni-15Sn (Fig. 5). Additionally, much lower oxidation was found on Cu-Ni-15Sn, when compared with Cu-Ni-10Sn and Cu-Ni (Fig. 12c and Table 5).

In fact, when analyzing Fig. 13, from (a) to (c), a clear transition on the wear track topography is found, from a softer (Cu-Ni) to a progressively harder (Cu-Ni-15Sn) material, promoted by the Sn content increase.

Regarding Cu-Ni-Sn-2WC wear track, large detachment zones along the sliding direction, having very low deepness, were found (Fig. 13d). The presence of WC particles in this material, having higher hardness, can substantially reduce the size and extent of grooves (Ref 20). Similar explanation can be given regarding Cu-Ni-Sn-10WC, once when analyzing Fig. 13(e), only minor grooves were found. In fact the main contribution of WC particles to wear is their load shearing ability, being a harder constituent than the matrix, thus preventing material loss by abrasion. It is also worth to notice that for both WC-reinforced materials, a good bond between the WC particles and the matrix was verified, due to no evidences of WC particles being pulled out from the matrix during sliding, but instead being retained and thus protecting the material from wear.

When comparing the chemical composition of similar areas on Cu-Ni-Sn-2WC and Cu-Ni-Sn-10WC wear tracks, some differences are found, pointing to a higher tendency for oxidation on Cu-Ni-Sn-10WC (see Table 4). Focusing on non-detached material areas (marked as Z2 on Fig. 12d and e), an expressively higher oxygen content is found for Cu-Ni-Sn-10WC. This difference can be explained by the fact that when a higher content of WC particles is added, severe abrasion is

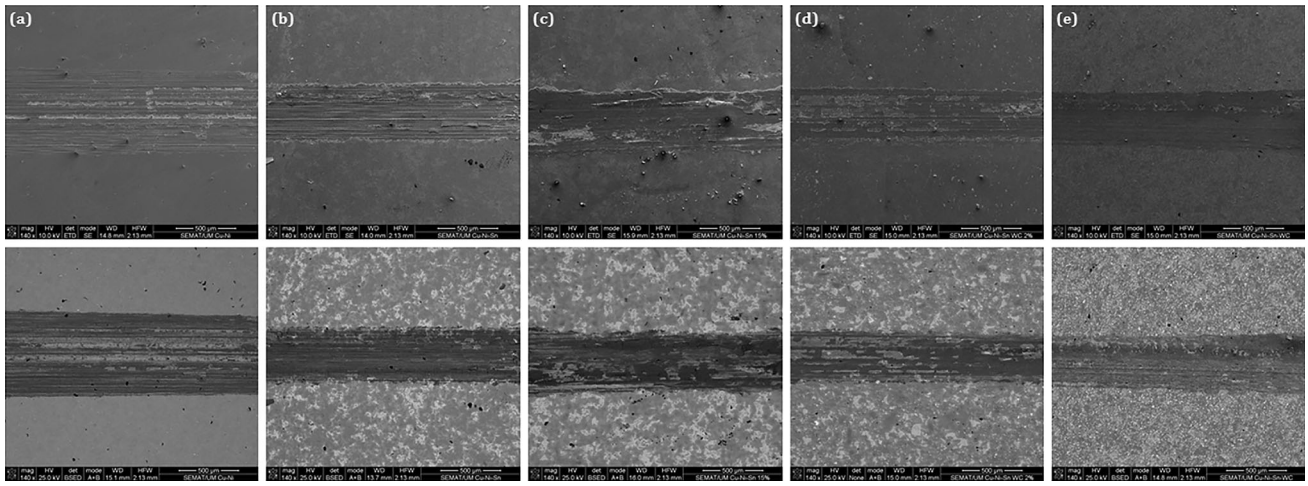

Fig. 11 Wear tracks of (a) Cu-Ni; (b) Cu-Ni-10Sn; (c) Cu-Ni-15Sn; (d) Cu-Ni-Sn-2WC and (e) Cu-Ni-Sn-10WC

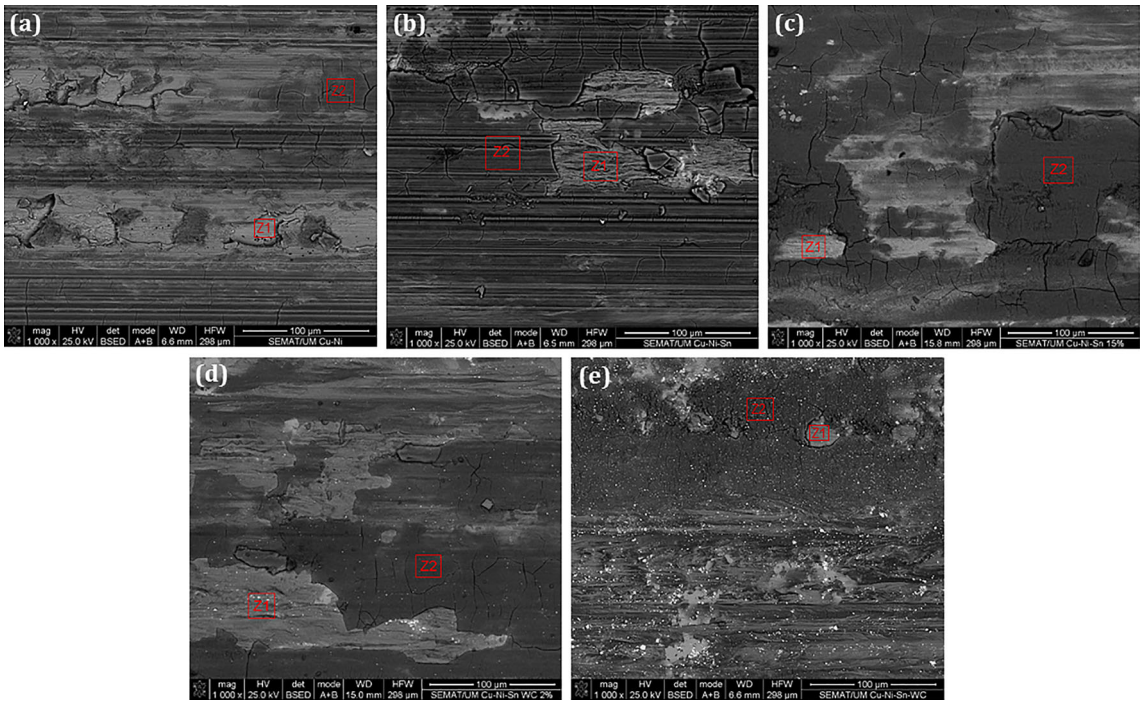

Fig. 12 BSED images of the wear tracks of (a) Cu-Ni; (b) Cu-Ni-10Sn; (c) Cu-Ni-15Sn; (d) Cu-Ni-Sn-2WC and (e) Cu-Ni-Sn-10WC, with marked zones for EDS analysis

avoided, but the non-detached material suffers more reciprocating motion, which due to local heating stimulates chemical reactions like oxidation.

Furthermore, there is a major difference between Cu-Ni-Sn-2WC and Cu-Ni-Sn-10WC wear tracks topography, once the latter presents deeper material detachment areas. This fact can be due to the presence of WC clusters, where the small WC particles are not perfectly bonded between them (due to agglomeration effect), acting as preferential sites for fracture during sliding. This is the main reason for the weight loss results obtained for Cu-Ni-Sn-10WC, shown in Fig. 9.

Table 5 Chemical composition of marked zones in Fig. 11, obtained by EDS

Composition, wt.%	Cu-Ni	Cu-Ni-10Sn	Cu-Ni-15Sn	Cu-Ni-Sn-2WC	Cu-Ni-Sn-10WC
Z1					
Cu	70.21	70.69	82.58	73.31	31.94
Ni	29.79	18.73	16.69	25.61	48.90
Sn	…	2.20	0.67	0.94	10.53
O	…	7.38	0.06	0.05	2.62
W	…	…	…	0.07	3.52
C	…	…	…	0.02	2.49
Al	…	…	…	…	…
Z2					
Cu	46.00	60.63	81.38	82.76	45.86
Ni	33.73	22.18	17.68	16.66	23.47
Sn	…	4.06	0.71	0.32	4.70
O	17.90	12.14	0.21	0.15	16.15
W	…	…	…	0.05	6.58
C	…	…	…	0.03	2.69
Al	2.37	1.09	0.02	0.03	0.54

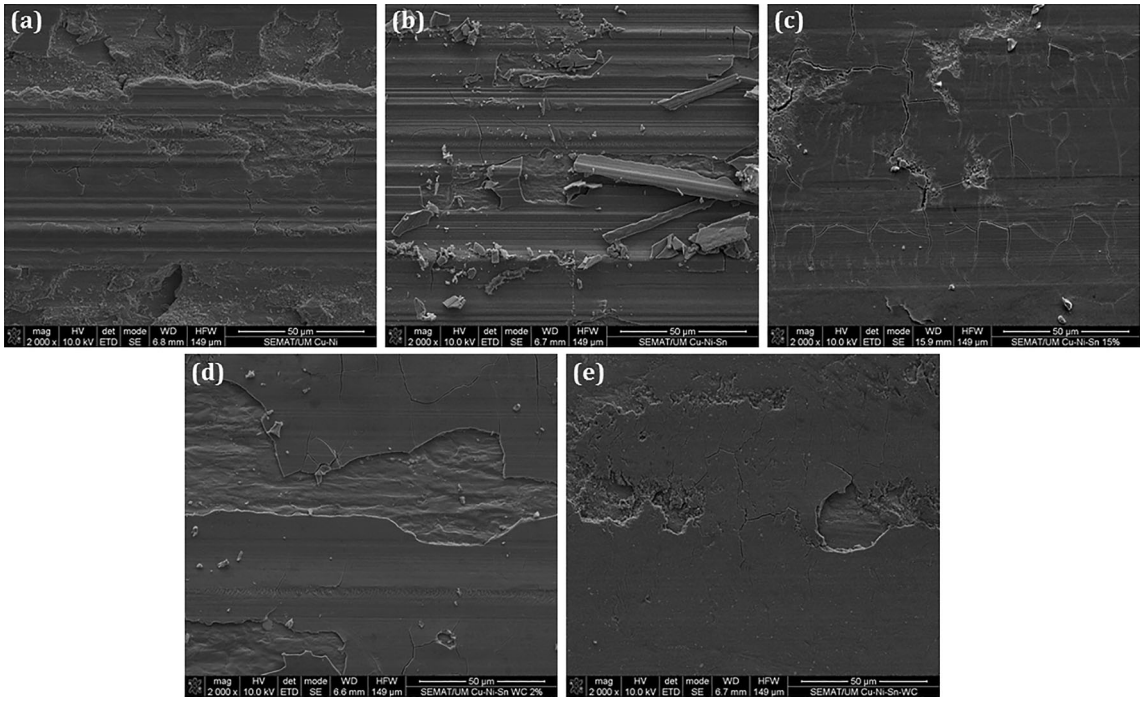

Fig. 13 SE images of the wear tracks of (a) Cu-Ni; (b) Cu-Ni-10Sn; (c) Cu-Ni-15Sn; (d) Cu-Ni-Sn-2WC and (e) Cu-Ni-Sn-10WC

4. Conclusions

The main conclusions that can be drawn from the work above described are:

- The production of Cu-Ni-based materials for using as matrix material for diamond cutting tools was successfully performed by hot-pressing technique, resulting in compacts with good densification;
- The addition of Sn to Cu-Ni alloy proved to be beneficial regarding the mechanical properties (hardness and shear strength) and also wear performance;
- Additions of 2%WC to Cu-Ni-Sn led to mechanical and wear performance improvement; however, higher WC additions (10%) led to comparatively inferior results;
- Among all the tested materials, the best compromise between mechanical and wear behavior was attained by Cu-Ni-10Sn and Cu-Ni-10Sn-2WC.

Acknowledgments

This work was supported by FTC (Fundação para a Ciência e a Tecnologia) through the grant SFRH/BPD/112111/2015 and the projects PTDC/EMS-TEC/5422/2014 and NORTE-01-0145-FED-

ER-000018-HAMaBICo and by CNPq-Brazil (PVE/CAPES/CNPq/407035/2013-3). Additionally, this work was supported by FCT with the reference project UID/EEA/04436/2013, by FEDER funds through the COMPETE 2020—Programa Operacional Competitividade e Internacionalização (POCI) with the reference project POCI-01-0145-FEDER-006941.

References

1. L.J. de Oliveira, G.S. Bobrovnitchii, and M. Filgueira, Processing and Characterization of Impregnated Diamond Cutting Tools Using a Ferrous Metal Matrix, *Int. J. Refract. Met. Hard Mater.*, 2007, **25**, p 328–335
2. K. Yamaguchi, N. Takakura, and S. Imatani, Compaction and Sintering Characteristics of Composite Metal Powders, *J. Mater. Process. Technol.*, 1997, **63**, p 364–369
3. J.N. Boland and X.S. Li, Microstructural Characterisation and Wear Behavior of Diamond Composite Materials, *Materials*, 2010, **3**, p 1390–1419
4. N.B. Dhokey, K. Utpat, A. Gosavi, and P. Dhoka, Hot-Press Sintering Temperature Response of Diamond Cutting Tools and Its Correlation with Wear Mechanism, *Int. J. Refract. Met. Hard Mater.*, 2013, **36**, p 289–293
5. B. Henriques, M. Gasik, G. Miranda, J.C.M. Souza, R.M. Nascimento, and F.S. Silva, Improving the Functional Design of Dental Restorations by Adding a Composite Interlayer in the Multilayer System: Multi-aspect Analysis, *Ciência & Tecnologia dos Materiais*, 2015, **27**, p 36–40
6. G. Miranda, M. Buciumeanu, S. Madeira, O. Carvalho, D. Soares, and F.S. Silva, Hybrid Composites—Metallic and Ceramic Reinforcements Influence on Mechanical and Wear Behavior, *Compos. Part B Eng.*, 2015, **74**, p 153–165
7. B. Henriques, G. Miranda, M. Gasik, J.C.M. Souza, R.M. Nascimento, and F.S. Silva, Finite Element Analysis of the Residual Thermal Stresses on Functionally Gradated Dental Restorations, *J. Mech. Behav. Biomed. Mater.*, 2015, **50**, p 123–130
8. G. Miranda, O. Carvalho, D. Soares, and F.S. Silva, Properties Assessment of Nickel Particulate Reinforced Aluminum Composites Produced by Hot Pressing, *J. Compos. Mater.*, 2016, **50**, p 523–531
9. N. Urakawa, et al., Cutting performance of bonded abrasive type diamond wire saw, in Proceedings of Intertech, Vancouver, 17–21 July 2000
10. J. Konstanty, *Powder Metallurgy Diamond Tools*, 1st ed., Elsevier, Amsterdam, 2005
11. J. Konstanty, Diamond Bonding and Matrix Wear Mechanisms Involved in Circular Sawing of Stone, *Ind. Diam. Rev.*, 2001, **60**, p 55–65
12. K. Przyklenk, Diamond Impregnated Tools—Uses and Production, *Toolmak. IDR*, 1993, **4**, p 192–195
13. M. Del Villar, P. Muro, J.M. Sánchez, I. Iturriza, and F. Castro, Consolidation of Diamond Tools Using Cu-Co-Fe Based Alloys as Metallic Binders, *Powder Metall.*, 2001, **44**, p 82–90
14. S.C. Cabral and M. Filgueira, Mecanismo de Desgaste em Matriz Ferrítica com Adição de Diamantes, *Revista Multidisciplinar do Nordeste Mineiro*, 2010, **2**, p 1–8
15. W. Tillmann, C. Kronholz, M. Ferreira, A. Knote, W. Theisen, P. Schütte, et al., Comparison of Different Metal Matrix Systems for Diamond Tools Fabricated by New Current Induced Short-Time Sintering Processes, in *Conference Proceedings Powder Metallurgy. 2010 World Congress, 2010*
16. L.J. de Oliveira and M. Filgueira, Pérolas Diamantadas Obtidas por Metalurgia do Pó: Nacionalização da Tecnologia, *Matéria (Rio J.)*, 2008, **13**, p 23–32
17. Z. Nitkiewicz and M. Świerzy, Tin Influence on Diamond–Metal Matrix Hot Pressed Tools for Stone Cutting, *J. Mater. Process. Technol.*, 2006, **175**, p 306–315
18. ASM Handbook Volume 2-Properties and Selection. Nonferrous Alloys and Special-Purpose Materials. ASM International 1990
19. P.K. Deshpande, J.H. Li, and R.Y. Lin, Infrared Processed Cu Composites Reinforced with WC Particles, *Mater. Sci. Eng. A*, 2006, **429**, p 58–65
20. J. Liu, S. Yang, W. Xia, X. Jiang, and C. Gui, Microstructure and Wear Resistance Performance of Cu-Ni-Mn Alloy Based Hardfacing Coatings Reinforced by WC Particles, *J. Alloys Compd*, 2016, **654**, p 63–70
21. J. Borowiecka-Jamrozek, Engineering Structure and Properties of Materials Used as a Matrix in Diamond Impregnated Tools, *Arch. Metall. Mater.*, 2013, **58**, p 5–8
22. M. Mészáros and K. Vadasdi, Process and Equipment for Electro-chemical Etching of Diamond-Containing Co-WC Tools and Recovery of Diamond from Used Steel Tools, *Int. J. Refract. Met. Hard Mater.*, 1996, **14**, p 229–234
23. B. Henriques, P. Ferreira, M. Buciumeanu, M. Fredel, A. Cabral, F.S. Silva, and G. Miranda, Copper-Nickel-Based Diamond Cutting Tools: Stone Cutting Evaluation, *Int. J. Adv. Manuf. Technol.*, 2017, doi: 10.1007/s00170-017-0220-6